

Systematic study of the stable states of C^- , Si^- , Ge^- , and Sn^- via infrared laser spectroscopy

Michael Scheer, René C. Bilodeau, Cicely A. Brodie, and Harold K. Haugen*

Department of Physics and Astronomy, McMaster University, Hamilton, Ontario, Canada L8S 4M1

(Received 24 April 1998)

The bound excited $np^3\ ^2D$ terms of Si^- , Ge^- , and Sn^- have been investigated with a combination of single- and multiphoton tunable infrared laser experiments. The binding energies of the two $J=3/2$ and $J=5/2$ fine-structure levels were found to be 0.527 234(25) and 0.525 489(20) eV, respectively for Si^- , 0.401 44(10) and 0.377 27(6) eV for Ge^- , and 0.397 617(15) and 0.304 635(15) eV for Sn^- . These results constitute improvements in accuracy over previous experimental term energies of up to four orders of magnitude and further provide experimental values for the 2D fine-structure splittings: 14.08(20), 192.6(9), and 749.95(15) cm^{-1} for Si^- , Ge^- , and Sn^- , respectively. In addition, the photodetachment thresholds of the ionic $^4S_{3/2}$ ground states have been reinvestigated. This resulted in improved electron affinities of 1.262 119(20), 1.389 521(20), 1.232 712(15), and 1.112 067(15) eV for C^- , Si^- , Ge^- , and Sn^- , respectively. Various attempts towards an observation of the very weakly bound $C^-(^2D)$ and $Si^-(^2P)$ terms remain unsuccessful. [S1050-2947(98)01910-6]

PACS number(s): 32.80.Gc, 32.80.Wr, 32.10.Fn

I. INTRODUCTION

Excited states of atomic negative ions that are bound with respect to the atomic ground state have long been considered as rare occurrences. For many ions, the experimental knowledge of such states is still poor, despite considerable effort over the past decades (see Refs. [1, 2] for recent reviews). Excited negative-ion states that are embedded as resonances in the energy continuum above the atomic ground state have been extensively studied with a variety of experimental techniques [3]. Most early investigations of bound excited states, on the other hand, were based on two techniques: laser photodetached electron spectrometry (LPES) and threshold photodetachment with conventional light sources. Both techniques are applicable to most stable negative ions, but the energy resolution is often insufficient for a determination of fine-structure splittings. The energy resolution achieved in laser photodetachment threshold (LPT) experiments is significantly higher and LPT studies of the more strongly bound O^- , S^- , Se^- , and Te^- ions have provided accurate values for the respective 2P fine-structure splittings [4]. LPT studies of weakly bound (<1 eV) ions are more challenging as they require tunable infrared laser sources. Nevertheless, accurate ionic fine-structure splittings have been obtained for Li^- [5] and recently also for B^- [6] and Al^- [7]. Both LPES and LPT studies have to rely on an initial population of the excited states to be investigated. This is generally not a constraint in measurements of the fine structure of the ionic ground state, as the corresponding level splittings are typically small. However, higher-lying excited terms or possibly electronically excited configurations would be only very weakly populated from a thermal ion source. In such cases, resonant multiphoton detachment may provide an alternative approach.

The interest in multiphoton phenomena involving negative ions began with the early demonstration of nonresonant two-photon detachment of I^- by Hall [8] and with the resonant two-photon detachment of C_2^- by Lineberger and Patterson [9]. Over the past few years, several other multiphoton phenomena have been observed in negative ions. Most studies investigated nonlinear optical processes such as excess-photon detachment [10], two-photon threshold detachment [11,12], and ponderomotive threshold shifts [13]. Negative ions represent qualitatively different targets for such strong-laser-field studies due to the absence of a Rydberg series of states, which is a result of the short-range potential that binds the extra electron of a negative ion. However, some multiphoton studies were aimed at the elucidation of negative-ion structure. Both bound excited states [14–16] and resonant structures in the continuum of negative-ion species [17,18] have been probed via multiphoton schemes. Bound excited negative-ion states almost always refer to the terms and fine structure of the same (ground-state) electronic configuration. Hence single-photon electric dipole ($E1$) transitions between such levels are strictly forbidden as a result of the parity selection rule. A simultaneous absorption of two photons, on the other hand, would be allowed in an electric dipole interaction and would give rise to a resonant enhancement in a multiphoton detachment spectrum. Recently, such a resonance has been observed in the single-color three-photon detachment spectrum of Sb^- [16] and previously in two-color detachment spectra of Se^- and Te^- where the two-photon bound-bound transition was realized in a Raman coupling scheme [14]. In addition to two-photon $E1$ transitions, small probabilities often exist for single-photon transitions of magnetic dipole ($M1$) or electric quadrupole ($E2$) character. Such “forbidden” transitions have recently been reported between fine-structure levels of Ir^- and Pt^- [15] and also between the fine-structure levels and terms of Sb^- [16]. In the latter case study of the antimony negative ion we have been able to demonstrate that a combination of resonant multiphoton techniques with traditional LPT spectroscopy can provide a complete knowledge of the stable states of an

*Also at Department of Engineering Physics, the Brockhouse Institute for Materials Research, and the Center for Electrophotonic Materials and Devices, McMaster University, Hamilton, Ontario, Canada L8S 4M1.

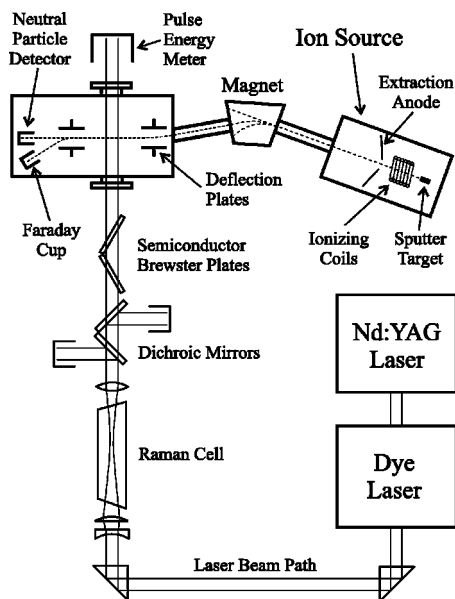


FIG. 1. Schematic diagram of the experimental setup (see the text for details).

atomic negative ion. It was the aim of the work described in the present article to systematically apply these techniques to the negative ions of the carbon group: C^- , Si^- , Ge^- , and Sn^- .

The anions of the carbon group elements have been considered particularly notable examples of negative ions with excited terms of the ground-state configuration that still lie below the first detachment threshold [1]. Nevertheless, the experimental knowledge of these excited terms is still rather limited, particularly for Ge^- and Sn^- where the relative experimental uncertainties are as large as 50%. In recent years, C^- , Si^- , and Ge^- have attracted considerable attention by theorists as well as experimentalists for their photodetachment cross section close to the $nsnp^3\ ^5S_2$ threshold, several eV above the first detachment threshold ($ns^2np^2\ ^3P_0$). Theoretical works [19] have predicted pronounced window resonances for these three ions, but experimental studies have found a resonance feature only in Si^- [20] and not in C^- [21] (to our knowledge, Ge^- has not yet been investigated in that respect).

II. METHODOLOGY

A. Experimental setup

The experimental apparatus that was utilized in the photodetachment studies described herein is comprised of a negative-ion source, an infrared laser source, and an ultrahigh vacuum (UHV) interaction chamber. The setup is schematically depicted in Fig. 1 and is described in detail in Ref. [22].

A Lumonics HD-300 dye laser is pumped by the second harmonic of a 10-Hz Q -switched Nd:YAG laser (where YAG denotes yttrium aluminum garnet), a Lumonics YM-800. Tunability over the (680–980)-nm region is achieved by utilizing a 1800-lines/mm grating and near-infrared dyes. Over this tuning range the ≈ 8 -ns laser pulses have a spectral bandwidth of 0.1 – 0.06 cm^{-1} . For wavelength conversion further into the infrared, the dye-laser beam is focused into a

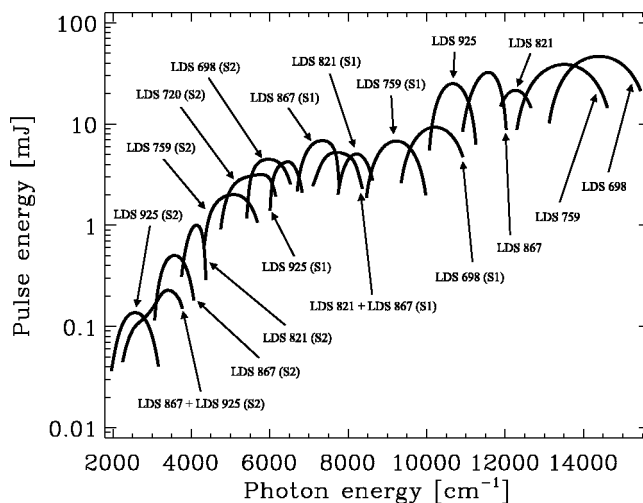


FIG. 2. Pulse energy curves for selected laser dyes and for the associated first and second Stokes conversions [indicated with the labels (S1) and (S2), respectively].

120-cm-long high-pressure hydrogen cell, where stimulated Raman scattering of the dye-laser light causes the generation of a first Stokes laser beam. In addition, coherent second Stokes and anti-Stokes radiation is emitted from the Raman cell as the result of parametric four-wave-mixing processes. Optogalvanic resonances of argon were utilized in a direct measurement of the first Stokes Raman shift. A value of $4155.197(20)\text{ cm}^{-1}$ was obtained, which agrees well with the literature value of $4155.187(5)\text{ cm}^{-1}$ [23] for a cell pressure of 22(1) bars. After the Raman cell, the beam is recollimated and then passed through dichroic mirrors to attenuate the undesired wavelength components by $\sim 90\%$ (anti-Stokes, residual pump, and also first Stokes radiation if second Stokes light is to be used). The final optical filtering is achieved with Brewster-angle pairs of silicon or germanium plates. This laser system allows for the production of tunable infrared laser light over the region of 1 – $5\ \mu\text{m}$ (see Fig. 2). Finally, the laser light passes through a CaF_2 viewport into the ultrahigh vacuum interaction chamber where it crosses the ion beam at 90° . The laser light is monitored with a pulse-energy meter located after the exit port of the chamber. In order to effectively eliminate absorption of the infrared light in air, the entire optics table and the pulse-energy meter can be sealed and purged with nitrogen gas.

Negative-ion beams are generated with a Middleton-type high-intensity cesium sputter source [24] and are accelerated to energies of 13 – 15 keV . For ions possessing more than one stable state, the relative population of these states depends on the effective temperature of the sputter surface. Depending on various ion source parameters, this temperature can be varied between approximately 500 and 1500 K . A 30° bending magnet with magnetic fields of up to 0.52 T serves to separate the atomic ion beam of interest from other atomic and molecular species. In order to minimize collisional detachment, the ion beam is passed through a differential pressure tube into an UHV chamber with background pressures of $\sim 10^{-8}\text{ mbar}$. There the beam is charge-state analyzed with a pair of electrostatic deflection plates, producing a deflection of 10° . The ions then enter a field-free region where they interact with the collimated or focused laser

beam. A second pair of electrostatic deflection plates is employed to deflect the residual negative ions into a Faraday cup, while the photodetached neutral atoms are detected with a discrete-dynode electron multiplier. The detector is operated in the analog regime, as the total number of detachment events per laser pulse is typically larger than one. After preamplification, the output signal of the detector is fed into a gated integrator and boxcar averager. A gate width of ~ 50 ns is usually sufficient to ensure that all the neutral particles produced during the laser pulse are collected. Such narrow gating very effectively reduces the number of collisional background events to ~ 1 count per pulse, per μA of beam current. Finally, the integrated signal for each pulse (or the average of a number of pulses) is recorded by a personal computer.

B. Data acquisition and analysis

A region of interest in the photodetachment cross section of a negative ion is typically investigated with a slow [(20–30)-min] dye-laser scan. Depending on the signal-to-noise ratio, the scan procedure is repeated up to ten times and individual scans are summed. A poor signal-to-noise ratio can be due to a large photodetachment background, small ion-beam currents, and/or low infrared pulse energies. Beam current and pulse energy are always recorded parallel to the neutral particle signal and are utilized to normalize the photodetachment data.

1. Threshold fit

A theoretical description of the relative cross section for photodetachment close to threshold is given by Wigner's threshold law [25]. It predicts a zero cross section for photon energies (ε) below the threshold energy (ε_0) and a cross section proportional to $(\varepsilon - \varepsilon_0)^{l'+1/2}$ for $\varepsilon > \varepsilon_0$, where l' denotes the angular momentum of the detached (i.e., free) electron. Hence detachment into an s -wave continuum exhibits a threshold with a sharp onset ($\sigma \propto \sqrt{\Delta\varepsilon}$), whereas the onset of a p -wave threshold is smooth ($\sigma \propto \Delta\varepsilon^{3/2}$). However, in most of the cases investigated here, the cross section displays a series of cascaded thresholds rather than just a single threshold. Hence, for an accurate fit to any particular threshold it is necessary to account for the effect of the other photodetachment channels. The contribution of these other channels to the total cross section in the vicinity of ε_0 will be smooth and can be represented by a linear term, as long as the respective thresholds are not too close to ε_0 . In this case, the function that is fitted to an individual s -wave threshold is given by

$$\sigma_0 = \begin{cases} a + b(\varepsilon - \varepsilon_0) + c_0\sqrt{\varepsilon - \varepsilon_0} & \text{for } \varepsilon > \varepsilon_0 \\ a + b(\varepsilon - \varepsilon_0) & \text{for } \varepsilon \leq \varepsilon_0. \end{cases} \quad (1)$$

The fitting routine that is utilized here performs a nonlinear least-squares fit via a multi-parameter gradient-expansion algorithm. The fitting parameters a , b , c_0 , and ε_0 are optimized simultaneously.

For a series of closely spaced thresholds the linear background approximation is not valid. In this case, all thresholds are fitted simultaneously. The fitted function is then defined recursively:

$$\sigma_n = \sigma_{n-1} + \begin{cases} c_n\sqrt{\varepsilon - \varepsilon_n} & \text{for } \varepsilon > \varepsilon_n \\ 0 & \text{for } \varepsilon \leq \varepsilon_n. \end{cases} \quad (2)$$

Here $n=0,1,2,\dots$ labels the individual thresholds in the series. Such a simultaneous fit is found to work well if only two or three thresholds are present and if their relative intensities are not too different. However, if several thresholds or thresholds with largely differing intensities have to be fitted, this fitting routine may fail to converge properly. In such a case, a sequential threshold fit is performed by fitting Eq. (1) to the lowest-energy threshold first, subtracting the fit from the data, then fitting the second threshold, again subtracting the fit from the data, and so on. This method is less rigorous than the simultaneous fit as the coupling between the fitting parameters is reduced. This may result in overoptimistic standard deviations in the fitted parameters, which are therefore verified on a case to case basis.

The range of validity of the Wigner law (1) is limited to the photodetachment cross section close to threshold. For a theoretical description of the cross section higher above threshold, correction terms have to be taken into account [26]. However, in cases where a deviation from the Wigner law is observed, an inclusion of higher-order terms to the fitting function (1) is avoided by restricting the final scan range to a region over which the Wigner law is valid. Generally, this does not result in an increased uncertainty of the fitted threshold value as the onset of an s -wave threshold is steep and well pronounced. In contrast, for p -wave detachment the cross section higher above threshold is often essential for a determination of the threshold value from a fit to the data [22,27].

Systematic deviations from the Wigner threshold behavior may also result from a (partial) saturation of the detachment process by the intense laser pulse. Partial saturation should not affect the near threshold data, i.e., the fitted threshold value, but it may have an effect on the measured relative threshold intensities, particularly if different thresholds are observed that originate from the same ionic level. In measurements of threshold strengths the linearity of detachment signal versus pulse energy is checked at the high-energy end of the scan range.

2. Threshold strength

The various photodetachment channels are associated with different electronic configurations, terms, or fine-structure levels in either the ion or the atom. The ions investigated here are stable only in the p^3 configuration. The resulting terms 4S , 2D , and 2P are well separated in energy, as are the 3P , 1D , and 1S terms of the p^2 configuration of the respective atoms. However, fine-structure splittings in both the atom and ion are small and will therefore give rise to closely spaced cascaded thresholds. Engelking and Lineberger [28] have presented a theory that quantifies the relative intensities of the various fine-structure transitions that constitute the photodetachment channels going from an ionic ^{2S+1}L term to an atomic $^{2S'+1}L'$ term. In this framework, the relative intensity of a fine-structure transition $J \rightarrow J'$ is given by

$$I(J, J') \propto \sum_{j=|l-1/2|}^{l+1/2} (2j+1)(2J+1)(2J'+1) \times \left\{ \begin{array}{ccc} S & L & J \\ \frac{1}{2} & l & j \\ S' & L' & J' \end{array} \right\}^2, \quad (3)$$

as long as the spin-orbit coupling of the electrons can be approximated by LS coupling and the ionic levels are statistically populated. Here l and j denote the orbital and total angular momentum of the bound electron that is to be detached. (It should be noted that the angular momentum l' of the detached electron is not relevant here, although it determines the shape of the threshold.) The selection rules for photodetachment are determined by the properties of the $9J$ symbol in Eq. (3):

$$|\Delta S| \leq \frac{1}{2}, \quad |\Delta L| \leq l, \quad |\Delta J| \leq l + \frac{1}{2}. \quad (4)$$

The ionic fine-structure levels are populated according to their statistical weights only if the level splittings are much smaller than kT , where T is the effective ion source temperature. If this is not the case, a Boltzmann factor $\exp[-E(J)/kT]$ must be included in Eq. (3) to account for a thermal population of the different energy levels. As Eq. (3) is derived on the basis of the LS -coupling approximation, a deviation between measured and calculated threshold intensities indicates the breakdown of this coupling scheme for the particular ion.

3. Resonances

As outlined in the Introduction, resonant multiphoton detachment constitutes an alternative to threshold detachment in the study of bound excited states. If a resonant enhancement in a multiphoton detachment spectrum is observed, an accurate determination of the corresponding excited level is rather straightforward. However, virtually all bound-bound transitions in atomic negative ions are single-photon $E1$ forbidden and therefore have only small transition probabilities of $M1$ and/or $E2$ character. The feasibility of the multiphoton approach for a particular excited state is therefore evaluated in a computer simulation of the laser-ion-beam interaction prior to the actual experiment. The simulation assumes a Lorentzian laser bandwidth and Gaussian profiles for the temporal and spatial shape of the laser beam as well as for the spatial shape of the ion beam. The number of detachment events per laser pulse is calculated as a function of the various ion and laser source parameters and as a function of estimated bound-bound and bound-free transition probabilities. Competing detachment channels such as single-photon detachment of the initial excited level population and non-resonant two-photon detachment of the ionic ground state are also included. It was found in the simulation as well as in the experiment that the success in driving a “forbidden” $(1+1)$ -photon detachment process often depends on the effective suppression of these competing channels. While a collimated laser beam gives rise to a large one-photon (excited-state) and only a very small two-photon (ground-state) detachment background, the situation is reversed for a tightly focused beam. Depending on the cross sections of the vari-

ous processes, the best resonant-signal-to-background-signal ratio may be obtained with one or the other beam geometry or an intermediate geometry such as a cylindrical focus.

4. Energy resolution

The resolution that can be achieved in photodetachment experiments with the present setup is limited by several factors. Most importantly, the finite bandwidth of the infrared laser source ($\approx 0.08 \text{ cm}^{-1}$) gives rise to a predominantly Lorentzian broadening of all spectroscopic features. Doppler effects may cause an additional Gaussian broadening. For the crossed-beam setup used here the angular divergence of the ion beam is the major source of Doppler broadening. Geometric considerations of the interaction chamber suggest that the beam divergence angle should not be more than 0.5° . In the case of photodetachment with visible light this angle may very well cause a Doppler broadening larger than the laser bandwidth, but for a typical infrared photodetachment experiment ($2\text{-}\mu\text{m}$ light, 15-keV beam energy, atomic mass of 60) a broadening of only 0.03 cm^{-1} results. Doppler broadening due to a (thermal) tangential velocity spread in the ion beam is even smaller and can therefore be neglected.

In principle, the finite interaction time between the fast ion beam and the pulsed laser beam constitutes an additional source of broadening. In practice, for a collimated laser beam this time is given by the duration of the laser pulse ($\approx 8 \text{ ns}$) and the resulting broadening is negligible. It is only for a tightly focused laser beam, as may be used in multiphoton detachment studies, that ion transfer times reach the subnanosecond regime and then cause broadenings of $\sim 0.1 \text{ cm}^{-1}$.

5. Systematic errors

In an attempt to minimize potential sources of systematic errors we have performed various tests with the infrared laser setup prior to the actual photodetachment experiments. Very well known transitions in argon [29] were used as a calibration standard for the tuning control unit of the dye laser. The calibrations were conducted with the aid of an argon-filled hollow cathode discharge lamp (Hamamatsu). Discharge lamps yield an optogalvanic effect, i.e., a measurable change in the discharge impedance whenever the laser wavelength is in resonance with certain atomic transitions of the filler gas [30]. Discharge lamps constitute a very convenient and quick means of wavelength calibration, but provide only relatively few calibration lines. There are 25 optogalvanically active transitions available within the (680–980)-nm dye-laser tuning range, with gaps between consecutive lines of up to 45 nm. Hence the wavelength calibration of most photodetachment experiments would have to rely on an extrapolation from the nearest argon lines, i.e., the calibration accuracy would strongly depend on the degree of nonlinearity in the tuning mechanism. Figure 3 shows differences between tabulated [29] and measured argon line positions in wave-number units. The lines span a wavelength range of 60 nm and were measured after the tuning control unit had been calibrated using only two lines. The data in Fig. 3 appear to fluctuate randomly about the zero line by small amounts of less than 0.05 cm^{-1} . However, the deviation of any particular line is reproducible ($\pm 0.01 \text{ cm}^{-1}$) in different measurements. The

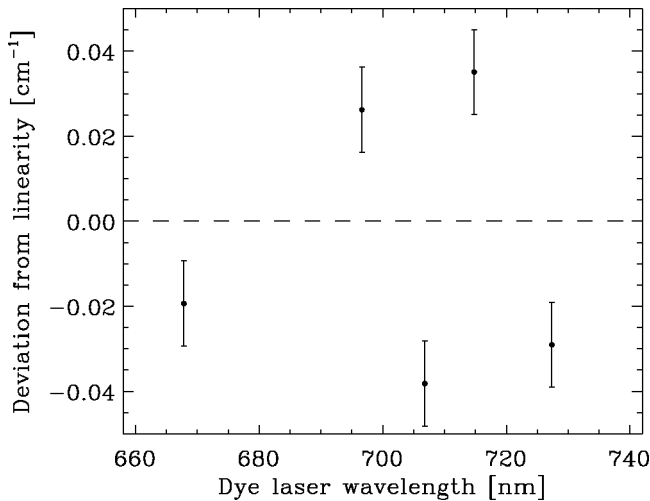


FIG. 3. Differences between measured and tabulated optogalvanic transitions in argon as a function of transition wavelength.

fluctuations are therefore believed to be the result of small ‘‘local’’ nonlinearities in the tuning mechanism. In order to determine an upper limit for this effect an étalon was employed to monitor the laser tuning over small regions (≈ 2 nm) at different wavelengths within the full tuning range. Deviations from linearity were very small, similar to those found for the argon lines. Therefore, a dye laser calibration uncertainty of 0.05 cm^{-1} is assumed for all experiments.

In addition to nonlinearities, possible temperature drifts are of some concern as certain threshold or resonance scans can take several hours. The dye laser was found to require a 2-hour warmup period before a drift of less than 0.01 cm^{-1} per hour is established. In addition to the water cooling of the laser dye, temperature gradients are minimized by continuously flushing the laser housing with cool nitrogen gas. A calibration performed on the temperature-stabilized laser would therefore remain valid throughout the experiment. The laser is recalibrated for each experiment to eliminate the possibility of small day-to-day fluctuations. In very long experiments that require the highest accuracy, laser calibrations are carried out before as well as after the detachment scans. This enables a correction of the data for possible wavelength drifts.

As a pulsed laser source is utilized, with peak intensities of $\sim 10^7$ and $\sim 10^{10} \text{ W/cm}^2$ for a collimated or focused beam, respectively, the possibility of intensity shifts has to be considered. The threshold for photodetachment in strong laser fields is shifted to higher energies due to the ponderomotive energy of a free electron in an electromagnetic field [13]. We have therefore investigated the ${}^4S_{3/2} \rightarrow {}^3P_0$ thresholds of C^- and Ge^- with a collimated laser beam (≈ 3 mm diameter), a cylindrically focused beam (25 cm focal length), and a spherically focused beam (20 cm focal length). While identical threshold values were obtained in the first two cases, a threshold shift of $\sim 1 \text{ cm}^{-1}$ resulted in the third case. To surely avoid possible intensity shifts, all photodetachment threshold experiments are conducted with collimated laser light. The bound-bound transition of a multiphoton detachment scheme, on the other hand, may be shifted in the presence of a strong laser field as a result of an ac Stark shift of

the negative-ion levels involved. However, for the transitions investigated here the ion levels belong to the same electronic configuration and should therefore exhibit very similar Stark shifts. Hence the transition energy should remain unshifted within experimental uncertainties. To be certain of this, we have measured the $\text{Sn}^-({}^4S_{3/2} \rightarrow {}^2D_{3/2})$ resonance (see Sec. III D) with the three aforementioned focusing geometries. No shifts in the resonance position were apparent.

A particular problem with the crossed-beam geometry of the present experimental setup is its susceptibility to linear Doppler shifts. In the rest frame of the fast ion beam the laser frequency will appear shifted whenever the crossing angle deviates from 90° . An alignment of this angle based on the geometry of the interaction chamber alone has an uncertainty of about 2° , necessitating further alignment checks. For a typical ion beam energy of 15 keV and a light element such as oxygen with an electron affinity of $11\,784.648(6) \text{ cm}^{-1}$ [1,31] a misalignment of 2° would result in a Doppler shift of 0.6 cm^{-1} . In addition to its extremely well known binding energy, O^- is also a very prolific ion from a Cs sputter source for almost any oxide cathode and furthermore detaches with a sharp s -wave threshold. Hence a detachment experiment with O^- provides a sensitive test for Doppler effects. A careful measurement of the $\text{O}^-({}^2P_{3/2} \rightarrow {}^3P_2)$ detachment threshold and a subsequent s -wave fit to the data resulted in a threshold value of $11\,784.62(3) \text{ cm}^{-1}$. The uncertainty given here represents the standard deviation obtained from the fitting routine and the calibration uncertainty for this particular wavelength range. Our value agrees with the more accurate literature value within one standard deviation. We therefore deduce an upper limit of 0.03 cm^{-1} for possible Doppler shifts due to laser beam misalignment. While the laser beam alignment is easily maintained between experiments, some uncertainty remains regarding small deviations in the beam path for different ions. Again, geometric considerations of the interaction chamber suggest that this uncertainty should not be more than 0.5° . Hence residual Doppler uncertainties are calculated on the basis of this value and the 0.03-cm^{-1} uncertainty from the O^- experiment. Final values range from 0.05 to 0.13 cm^{-1} depending on atomic mass and photon energy.

Finally, the uncertainty in the Raman shift has to be accounted for whenever first or second Stokes radiation is employed. Values of 0.02 and 0.04 cm^{-1} are used, respectively, based on the uncertainty of our experimentally determined Raman shift (see Sec. II A). The uncertainties of the final experimental results given in this paper always include these various systematic errors in addition to the standard deviations obtained from the numerical fits to the data.

III. RESULTS AND DISCUSSION

A. Carbon

Despite the fact that carbon is a light (first-row) element, there have been very few experimental investigations of its negative ion. The binding energy of the ionic $2p^3 {}^4S_{3/2}$ ground state was measured via LPES by Bennett and Hall [32] and via infrared LPT by Feldmann [33]. They obtained values of $1.268(5) \text{ eV}$ and $1.2629(3) \text{ eV}$, respectively. Feldmann used a laser-pumped optical parametric oscillator for his pioneering infrared LPT work. In addition to the ground-

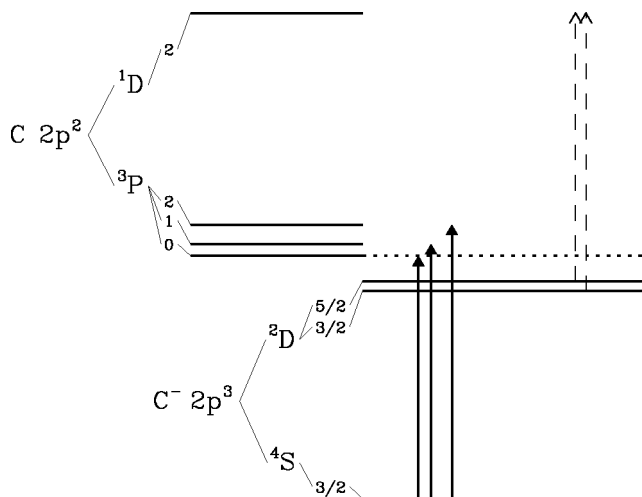


FIG. 4. Schematic energy-level diagram of C^- and C . Arrows indicate detachment thresholds, ordered by threshold energy. The horizontal spacing between arrows is proportional to the energy separation of the respective thresholds. Only the ${}^4S_{3/2} \rightarrow {}^3P_{J'}$ thresholds (solid arrows) could be measured in the present study. For clarity of presentation, fine-structure splittings are not shown to scale.

state detachment thresholds, his LPT spectrum also provided evidence for an ionic $2p^3 {}^2D$ term with a binding energy of 33(1) meV, which agreed with earlier values of 37(3) meV and 50(20) meV, obtained via field ionization measurements [34] and LPES [32], respectively. Based on these previous investigations, the energy level structure of C^- and the order of photodetachment thresholds are depicted in Fig. 4.

Since the recent LPT studies of Li^- [35] and B^- [6], carbon has become the first-row element with the largest uncertainty in its electron affinity, 0.3 meV (versus 0.025 meV for B^-). Many calculations of the electron affinity (EA) of carbon have been performed to date [36], but they typically exhibit errors of several meV. On the other hand, recent large-scale multiconfiguration Hartree-Fock calculations of the EA of lithium [37] and boron [38] have indicated that calculation errors of less than 1 meV might be achievable in future *ab initio* calculations of other first-row elements. Hence a more accurate determination of the EA of carbon seems appropriate.

We have investigated the photodetachment cross section of C^- over the photon energy range of 10 160–10 580 cm^{-1} or 1.260–1.312 eV [1 eV=8065.5410(24) cm^{-1} [39]]. The region that exhibits the three ${}^4S_{3/2} \rightarrow {}^3P_{J'}$ thresholds is shown in Fig. 5. As can be seen, the thresholds follow the Wigner s -wave behavior very closely (solid line). The ratio of measured transition strengths, 0.9:3.1:5.0, agrees well with the ratio of statistical weights for the fine-structure levels of the atomic ground state, 1:3:5. The intervals between the three thresholds are 16.3(2) and 26.8(2) cm^{-1} , also in good agreement with tabulated values for the fine-structure splittings of the atom, 16.40 and 27.00 cm^{-1} , respectively [40]. A high-resolution scan of the EA-defining ${}^4S_{3/2} \rightarrow {}^3P_0$ threshold is shown in Fig. 6. The scan range of 2.4 cm^{-1} corresponds to one standard deviation of the earlier result by Feldmann [33]. The observed photodetachment cross section deviates from the ideal Wigner s -wave behavior (dashed line), primarily due to the finite laser bandwidth of

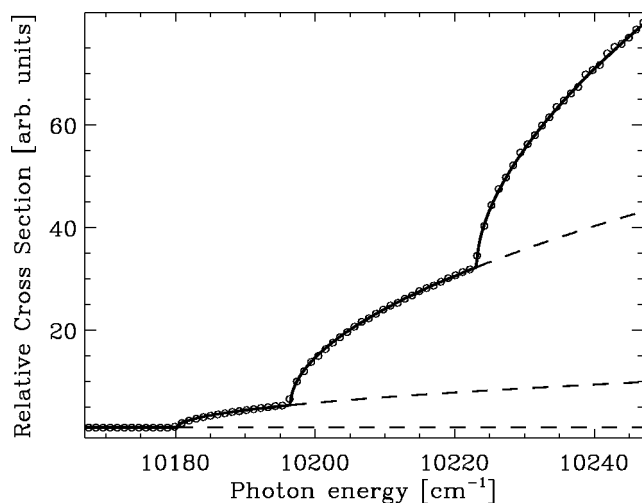


FIG. 5. Measured photodetachment cross section of C^- in the region of the ${}^4S_{3/2} \rightarrow {}^3P_{J'}$ thresholds. The result of a Wigner s -wave fit to the data is indicated by the solid line. Individual thresholds are extrapolated with dashed lines.

$\leq 0.1 cm^{-1}$. In addition, a small modulation of the cross section is apparent, which results from the presence of a weak electrostatic field. Although the current design of the UHV interaction chamber provides for a shielding of the electrostatic deflection plates, stray fields of ~ 10 V/cm seem to remain. Fortunately, the effect of static electric fields on s -wave thresholds has been thoroughly investigated in the past [41] and can be accurately modeled with a theory presented by Baruch *et al.* [42]. If the cross section obtained with this model is convoluted with a Lorentzian bandwidth function, the solid line in Fig. 6 is obtained. The excellent agreement between fitted and measured cross sections allows for an accurate determination of the threshold energy: 10 179.67(15) cm^{-1} [1.262 119(20) eV]. The uncertainty given here includes possible systematic errors in the calibration or due to Doppler shifts (see Sec. II B 5). It is important

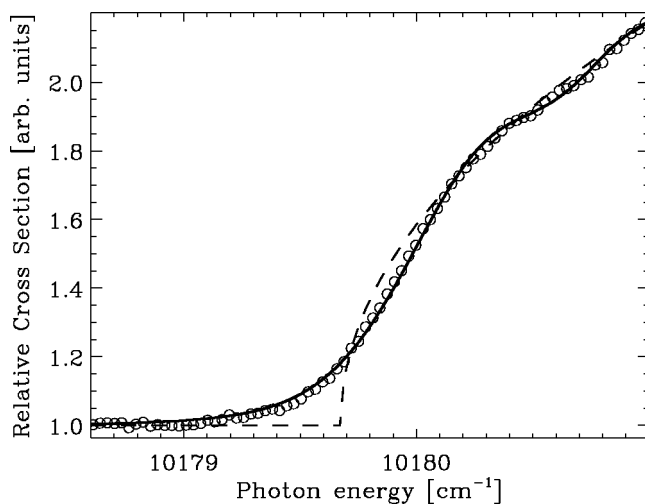


FIG. 6. High-resolution scan of the C^- detachment cross section in the vicinity of the ${}^4S_{3/2} \rightarrow {}^3P_0$ threshold. An ideal Wigner s -wave fit is indicated by the dashed line, while the result of an s -wave fit that includes bandwidth and field effects is represented by the solid line.

to note that the same threshold value is obtained if the effects of laser bandwidth and electric field are ignored in the fit (dashed line in Fig. 6). Hence the Wigner s -wave fit (1) remains valid.

Our value improves the accuracy of the EA of carbon by a factor of 15, but the value lies outside the error margin of Feldmann's result of 1.2629(3) eV [33]. This seems to indicate that a source of systematic error unaccounted for might have been present in the earlier work.

In an attempt to reproduce the weak ${}^2D_J \rightarrow {}^1D_2$ threshold feature observed by Feldmann, we have carefully investigated the detachment cross section in the (945–965)-nm range, which corresponds to 2D binding energies between 21 and 48 meV. No evidence for a threshold structure was found. There can be no doubt about the existence of the ${}^2D_J \rightarrow {}^1D_2$ thresholds, as the positive 2D binding energy was confirmed in five independent studies [32–34,43,44]. Hence an insufficient population of the 2D_J levels from our ion source is the most likely explanation for the absence of the corresponding threshold features. Nonthermal population mechanisms cannot be ruled out for a sputter ion source, but if we assume a mainly thermal population, less than 0.1% of the ions would be produced in the excited 2D_J states. Thus a signal-to-noise ratio of better than 1000 would be required for an unambiguous observation of the ${}^2D_J \rightarrow {}^1D_2$ thresholds, due to the substantial photodetachment signal from the ionic ground state. In the study of Feldmann the ions were produced via a discharge, which likely resulted in a higher 2D population. Recent LPES studies of the C^- detachment cross section at 2.076 eV have shown that a fractional 2D population of 50% can be achieved if the C^- beam is produced by charge exchanging a C^+ beam [43,44]. Hence a combination of this beam generation technique and infrared LPT (and possibly state-selective detection) should enable an accurate determination of the two $C^-({}^2D_J)$ levels.

B. Silicon

The energy level structure of Si^- , which is schematically shown in Fig. 7, is similar to that of C^- , with the interesting difference that for Si^- both the 2D and the 2P excited terms of the p^3 configuration are bound with respect to the atomic ground state. Early indications for this scenario were confirmed in an LPES study by Kasdan *et al.* [46], which determined 2D and 2P binding energies of 523(5) and 29(5) meV, respectively. For the 2P term a binding energy of 35(4) meV was also obtained by Oparin *et al.* in a field ionization measurement [34]. To our knowledge, none of the previous studies of these bound ionic terms have been able to resolve the respective fine structure. The binding energy of the ${}^4S_{3/2}$ ionic ground state, i.e., the electron affinity of silicon, is well known from the LPES experiment of Kasdan *et al.* [1.385(5) eV [46]] and more accurately from our previous infrared LPT study of this system, which yielded 1.389 49(6) eV [47]. Since improved calibration procedures now allow us to measure EA's with uncertainties as small as 0.01 meV, we decided to reinvestigate the EA-defining ${}^4S_{3/2} \rightarrow {}^3P_0$ threshold. (A determination of excited-state binding energies via bound-bound resonances hinges on an accurately known EA; see below.) A high-resolution scan over the (11 205–11 211)- cm^{-1} photon energy range

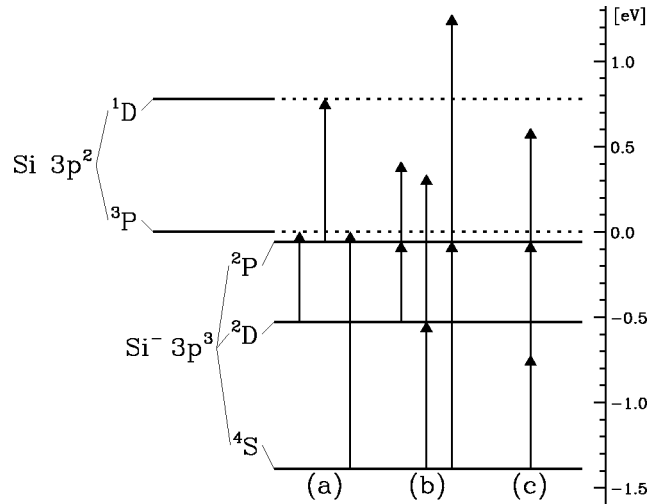


FIG. 7. Schematic energy-level diagram of Si^- and the Si ground state. Arrows indicate the various detachment schemes that were attempted in the present study: (a) one-photon threshold detachment, (b) resonant two-photon detachment via one-photon $M1$ or $E2$ transitions, and (c) resonant three-photon detachment via two-photon $E1$ transitions. For simplicity, fine-structure splittings are not shown.

yielded a threshold energy of 11 207.24(15) cm^{-1} [1.389 521(20) eV], in good agreement with our earlier value. A strong photodetachment background indicated a useful population of the excited ion levels, approximately a few nA out of the 2 μA total Si^- current. Hence an observation of the actual ${}^2D_J \rightarrow {}^3P_J$ thresholds seemed possible. A subsequent scan over a photon energy range of 4200–4500 cm^{-1} , shown in Fig. 8, revealed five nested thresholds. We attempted to fit the data over the full range shown using the Wigner s -wave law and its leading correction term [26] (solid line in Fig. 8). As can be seen, the data deviate from the predicted threshold behavior already after the third threshold (${}^2D_{3/2} \rightarrow {}^3P_1$). Similar deviations were

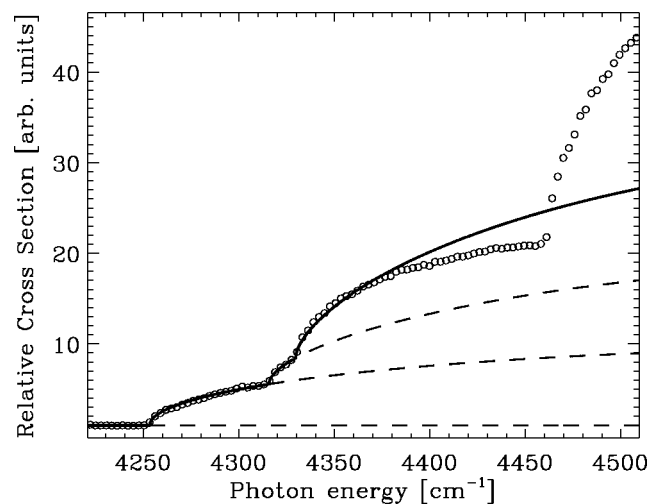


FIG. 8. Measured photodetachment cross section of Si^- in the region of the ${}^2D_J \rightarrow {}^3P_J$ thresholds. For the first three thresholds the result of a Wigner s -wave fit including the leading correction term is indicated by the solid line. Individual thresholds are extrapolated with dashed lines.

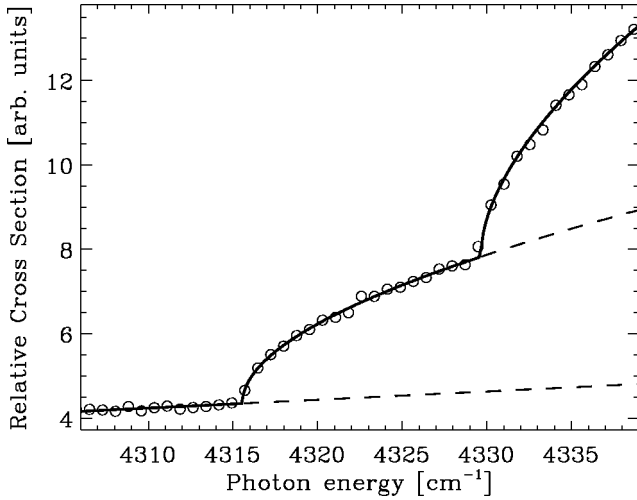


FIG. 9. Si^- photodetachment data in the vicinity of the ${}^2D_J \rightarrow {}^3P_1$ thresholds.

previously observed for Al^- photodetachment thresholds [7,48]. Hence an accurate determination of threshold energies and strengths had to rely on the near-threshold data alone. The regions of the ${}^2D_J \rightarrow {}^3P_1$ and ${}^2D_J \rightarrow {}^3P_2$ thresholds were therefore rescanned with higher resolution. The results are shown in Figs. 9 and 10, respectively. Threshold energies and strengths that were obtained from a Wigner s -wave fit to these data sets (where the background was approximated linearly) are summarized in Table I. Calculated threshold strengths (3) are given for comparison. Separations between thresholds of $77.11(25) \text{ cm}^{-1}$ for ${}^2D_{3/2} \rightarrow {}^3P_{0,1}$ and $145.92(20) \text{ cm}^{-1}$ for ${}^2D_{5/2} \rightarrow {}^3P_{1,2}$ were found, in good agreement with 77.115 and 146.042 cm^{-1} , respectively, the tabulated values for the fine-structure splittings of the $\text{Si}(3p^2 \ ^3P)$ term [40]. This proves that detachment to the atomic ground state is observed. The presence of a 2D term as the initial ionic state is evident from the good agreement between measured and calculated threshold strengths, in particular from the absence of the ΔJ -forbidden ${}^2D_{5/2} \rightarrow {}^3P_0$ threshold. The $\text{Si}^-({}^2D_J)$ binding energies that can be extracted from the threshold values are $4252.43(20)$ and

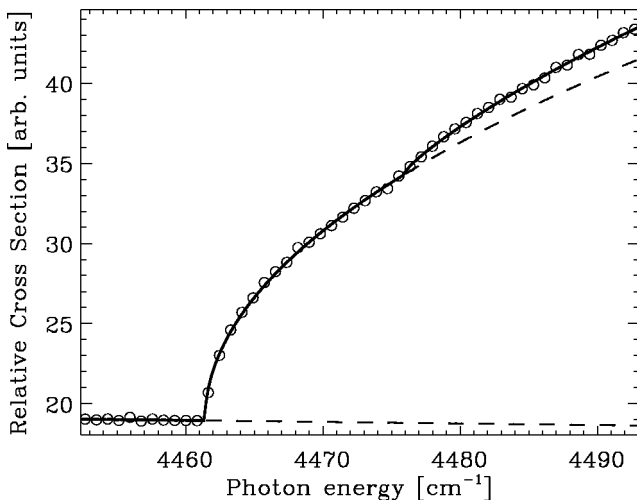


FIG. 10. Photodetachment cross section of Si^- in the ${}^2D_J \rightarrow {}^3P_2$ threshold region.

TABLE I. Results of the s -wave fits to the Si^- photodetachment data.

Transition	Threshold		Relative strength	
	Energy (cm^{-1})	Measured	Measured	Calculated
${}^2D_{5/2} \rightarrow {}^3P_0$	a	a	0	
${}^2D_{3/2} \rightarrow {}^3P_0$	4252.43(25)	10(1)	10	
${}^2D_{5/2} \rightarrow {}^3P_1$	4315.53(20)	11(1)	9	
${}^2D_{3/2} \rightarrow {}^3P_1$	4329.54(20)	19(2)	21	
${}^2D_{5/2} \rightarrow {}^3P_2$	4461.45(15)	45(2)	45	
${}^2D_{3/2} \rightarrow {}^3P_2$	4475.7(5)	5(1)	5	

^aThis transition is forbidden by the ΔJ selection rule.

$4238.35(15) \text{ cm}^{-1}$ [$527.234(25)$ and $525.489(20) \text{ meV}$] for $J=3/2$ and $J=5/2$, respectively. These values compare well with the average binding energy of $523(5) \text{ meV}$ measured by Kasdan *et al.* [46]. The difference between our two values gives a 2D fine-structure splitting of $14.08(20) \text{ cm}^{-1}$, which is in disagreement with $7(2) \text{ cm}^{-1}$, a value that was obtained earlier from isoelectronic extrapolation [45].

The very small binding energy of the $\text{Si}^-({}^2P)$ term precludes a determination of the detachment thresholds to the atomic ground state. The thresholds for detachment to $\text{Si}(3p^2 \ ^1D_J)$ would be within the tuning range of the present infrared laser source, but would suffer from a very unfavorable signal-to-background ratio, similar to the ${}^2D_J \rightarrow {}^1D_2$ thresholds in C^- (Sec. III A). We have therefore attempted to probe the 2P_J levels via resonant multiphoton detachment. The various possibilities for resonant multiphoton detachment from Si^- are shown in Fig. 7. Probabilities for single-photon bound-bound transitions can be extrapolated from calculated Einstein A coefficients for the phosphorous isoelectronic sequence [49]. The number of detachment events per laser pulse is then evaluated with a computer simulation of the laser-ion-beam interaction (as described in Sec. II B 3). The results obtained for Si^- are summarized in Table II. Depending on scan speed and background counts, signal enhancements as small as 0.1 events per pulse can be detected with the present setup. We have therefore searched for the ${}^4S_{3/2} \rightarrow {}^2P_J$ resonances over a 30-meV-wide photon energy range ($10\,841$ – $11\,093 \text{ cm}^{-1}$), which covers a 3σ error

TABLE II. Estimated probabilities for single-photon bound-bound transitions in Si^- .

Transition		Rate	
Levels	Type ^a	A (s^{-1})	Counts/pulse ^b
${}^4S_{3/2} \rightarrow {}^2P_{3/2}$	$M1^c$	0.005	3
${}^4S_{3/2} \rightarrow {}^2P_{1/2}$	$M1^c$	0.002	1
${}^2D_{3/2} \rightarrow {}^2P_{3/2}$	$E2$	0.008	0.06
${}^2D_{3/2} \rightarrow {}^2P_{1/2}$	$E2$	0.013	0.1
${}^2D_{5/2} \rightarrow {}^2P_{3/2}$	$E2$	0.016	0.2
${}^2D_{5/2} \rightarrow {}^2P_{1/2}$	$E2$	0.008	0.1

^aOnly the dominant character of the transition is indicated.

^bCounts/pulse are calculated for a focal spot size of 0.1 mm and a bound-free cross section of 10^{-17} cm^2 .

^cThese transitions violate the ΔS and ΔL selection rules. This reduces the accuracy of isoelectronic extrapolation.

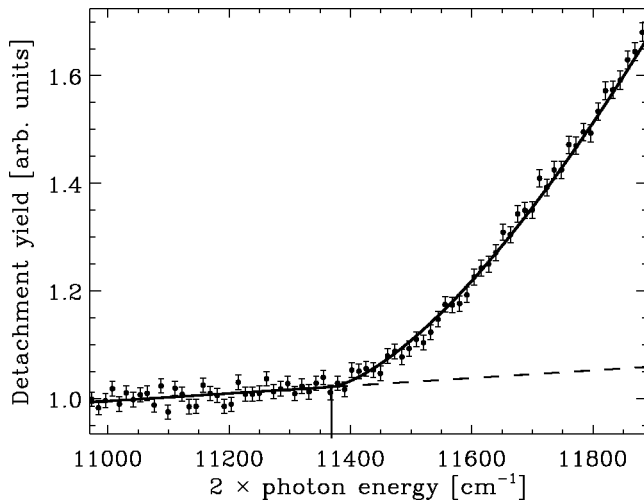


FIG. 11. Measured two-photon $\text{Si}^{-}(^4S_{3/2}) \rightarrow \text{Si}(^3P)$ detachment threshold. The solid line shows the result of a Wigner p -wave fit to the data.

margin of the 2P binding energy measured by Kasdan *et al.* [46]. No resonant features were apparent in this scan (which was conducted at a rate of 1000 laser pulses per cm^{-1}). The resonances could be somewhat weaker than the estimates suggest and would then likely be hidden in the substantial $\text{Si}^{-}(^2D)$ detachment background of ~ 50 counts per pulse. Similarly, a search for the $^2D_J \rightarrow ^2P_J$ resonances over the $(3925\text{--}4090)\text{-cm}^{-1}$ range with the same scan rate remained unsuccessful. The photodetachment background was much smaller in this case, but so were the estimated resonance signals (Table II). Most importantly, the background signal due to collisions of the Si^{-} ions with rest gas molecules in the UHV chamber was very high (~ 1 event/pulse). This collisional background is due to the large ($\approx 1 \mu\text{A}$) Si^{-} beam current and is likely responsible for the absence of the expected resonance features. As for $\text{C}^{-}(^2D)$, these complications could be avoided in future experiments if different ion-beam techniques such as charge exchange, an improved UHV system, and/or state-selective detection schemes were employed.

An alternative to driving a particular transition via an $E1$ -forbidden one-photon absorption is the possibility of $E1$ -allowed two-photon absorption. Since the $\text{Si}^{-}(^2P_J)$ levels are only weakly bound, the $^4S_{3/2} \rightarrow ^2P_J$ two-photon resonances are expected to lie just below the $^4S_{3/2} \rightarrow ^3P_0$ two-photon detachment threshold. This threshold was investigated first in order to optimize the focusing geometry for higher-order processes. The result is shown in Fig. 11. The threshold for two-photon detachment at $11\,370(15)\text{ cm}^{-1}$ and the expected p -wave threshold behavior are apparent. (A two-photon p -wave threshold has been previously observed in Cl^{-} detachment [11].) The observed threshold value compares well with $11\,357\text{ cm}^{-1}$, the average threshold value for an unresolved $\text{Si}(^3P)$ fine structure (although a ponderomotive threshold shift of a few cm^{-1} may be present). At energies below the two-photon threshold a small photodetachment signal is observed. This signal results from one-photon detachment of $\text{Si}^{-}(^2D)$ and from three-photon detachment of $\text{Si}^{-}(^4S)$. However, our final search for the $^4S_{3/2} \rightarrow ^2P_J$ two-

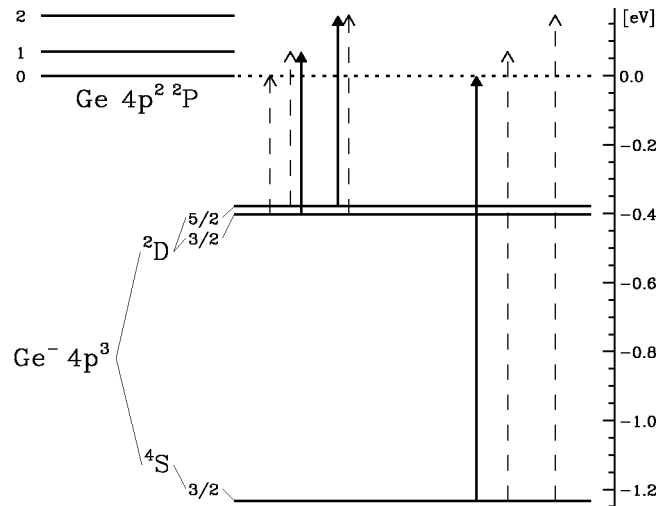


FIG. 12. Schematic energy-level diagram of Ge^{-} and the Ge ground state. Arrows indicate expected photodetachment thresholds in order of increasing photon energy. Thresholds that were observed are shown with solid arrows; others are dashed.

photon transitions over the $(5590\text{--}5400)\text{-cm}^{-1}$ photon energy range (at a rate of 500 pulses/ cm^{-1}) revealed no resonant enhancements over the detachment background. The absence of any resonance structure is likely due to a very small transition probability. The transitions would be “spin forbidden” and although we previously succeeded in driving a spin-forbidden two-photon transition in the case of Sb^{-} [16], a spin change is a much more serious constraint for a transition in a light system that is well described by LS coupling, such as Si^{-} .

C. Germanium

An energy level diagram for Ge^{-} and the Ge ground state is presented in Fig. 12. Accurate $\text{Ge}^{-}(^4S_{3/2})$ binding energies (EA of Ge) of $1.233(3)\text{ eV}$ and $1.232\,73(5)\text{ eV}$ were previously obtained in LPES [50] and infrared LPT [47] studies, respectively. As with Si^{-} , we have reinvestigated the $^4S_{3/2} \rightarrow ^3P_0$ photodetachment threshold of Ge^{-} in the present study. An improved value for the EA of Ge was obtained: $9942.49(12)\text{ cm}^{-1}$ [$1.232\,712(15)\text{ eV}$], in good agreement with the previous values.

In contrast to the Ge^{-} ground state, there has been only one previous observation of the excited $\text{Ge}^{-}(^2D)$ term, which was reported by Feldmann *et al.* [51]. Their photodetachment threshold experiment employed a conventional light source and indicated a low-energy threshold at 0.4 eV , which was attributed to detachment from $\text{Ge}^{-}(^2D)$. No uncertainties are given in the original paper, but the result is referenced in the 1985 Hotop-Lineberger tables [4] with an uncertainty of 0.2 eV , which seems consistent with the typical errors of that experimental technique. Based on this average 2D binding energy, the five $^2D_J \rightarrow ^3P_J$ thresholds would be expected in the $(1800\text{--}6200)\text{-cm}^{-1}$ photon energy range, spread out over $\sim 1400\text{ cm}^{-1}$. Using the isoelectronically extrapolated value of $160(30)\text{ cm}^{-1}$ for the 2D fine-structure splitting [45], the thresholds would appear in the order shown in Fig. 12. A scan of the $(3184\text{--}5975)\text{-cm}^{-1}$ range revealed only two weak s -wave threshold features at

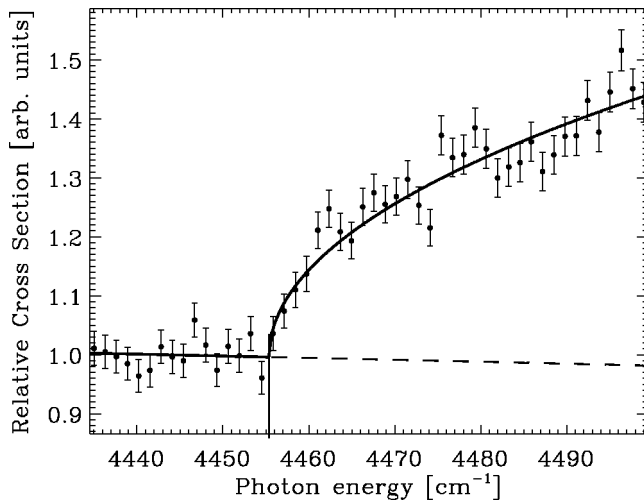


FIG. 13. Measured photodetachment cross section of Ge^- in the region of the ${}^2D_{5/2} \rightarrow {}^3P_2$ threshold. The result of a Wigner s -wave fit to the data is indicated by the solid line. Error bars are estimated on the basis of counting statistics.

3795.0(8) and 4455.3(5) cm^{-1} , the latter of which is shown in Fig. 13. The substantially smaller signal compared to the equivalent experiment with Si^- must be attributed to the much lower total ion-beam current available here (≈ 100 nA). The signal obtained for the threshold at 3795 cm^{-1} was in fact close to the detection limit of the apparatus. Since the two thresholds are separated by 660.3(9) cm^{-1} , which does not match with any separation between the $\text{Ge}({}^3P_J)$ levels (0, 557.1341, and 1409.9609 cm^{-1} for $J=0, 1,$ and $2,$ respectively [40]), the thresholds must originate from different ionic levels. The only reasonable assignment for the two thresholds seems to be ${}^2D_{3/2} \rightarrow {}^3P_1$ and ${}^2D_{5/2} \rightarrow {}^3P_2$, respectively. With this assignment, an ionic fine-structure splitting of 192.6(9) cm^{-1} is obtained, which falls within a 2σ error margin of the isoelectronic value of 160(30) cm^{-1} . Any other assignment would result in a negative splitting or in an unreasonably large value of 660 cm^{-1} or more. The two assigned thresholds also happen to be the strongest thresholds in the series, which would suggest that the signal from the three remaining thresholds was simply too small for detection with the current setup. We therefore conclude that the ${}^2D_{3/2}$ and ${}^2D_{5/2}$ levels of Ge^- are bound by 3237.9(8) and 3045.3(5) cm^{-1} [401.44(10) and 377.57(6) meV], respectively. Unfortunately, a confirmation of these level energies via resonant multiphoton detachment is rather challenging, considering the very small ${}^2D_{3/2,5/2} \rightarrow {}^4S_{3/2}$ transition probabilities of 0.01 and 0.0005 s^{-1} (extrapolated from calculated isoelectronic values [52]). Attempts to drive the ${}^4S_{3/2} \rightarrow {}^2D_{3/2}$ $M1$ transition remain unsuccessful.

D. Tin

As for Ge^- , the ${}^4S_{3/2}$ ground state of Sn^- has been accurately measured in two previous studies. Miller *et al.* [50] obtained a binding energy of 1.112(4) eV from LPES data, while an infrared LPT study by Thøgersen *et al.* [47] yielded 1.112 09(6) eV. Our initial experiments with Sn^- were aimed at a confirmation of this EA value. A high-resolution scan provided a threshold value of 8969.42(12) cm^{-1}

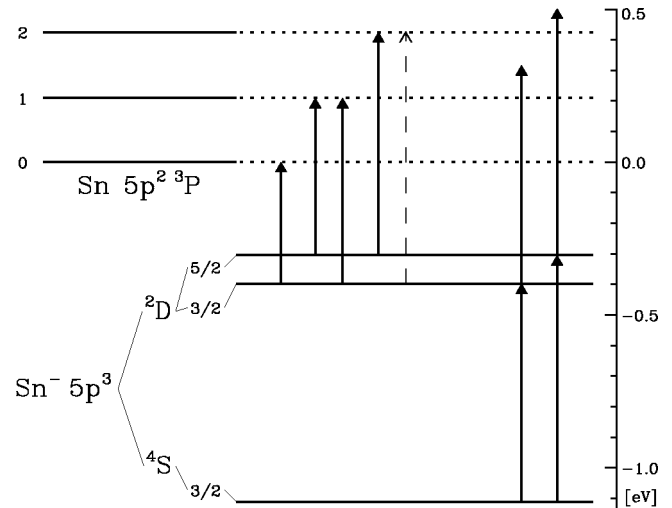


FIG. 14. Schematic energy-level diagram of Sn^- and the Sn ground state. Arrows indicate ${}^2D_J \rightarrow {}^3P_{J'}$ photodetachment thresholds and resonant two-photon detachment schemes. For simplicity, ${}^4S_{3/2} \rightarrow {}^3P_{J'}$ thresholds are not shown.

[1.112 067(15) eV] for the EA-defining ${}^4S_{3/2} \rightarrow {}^3P_0$ transition, in excellent agreement with the earlier works. The ~ 300 -nA Sn^- beam employed here was derived from a solid metal sputter cathode. This cathode was found to perform very poorly at higher effective sputter temperatures, which are essential for efficient detachment from excited ionic levels. As a result, 2D detachment signals were disappointingly small.

Unfortunately, the previous experimental knowledge of the $\text{Sn}^-({}^2D)$ term is even less established than in the case of Ge^- . Again, the only previous investigation is the photodetachment study of Feldmann *et al.* [51]. Photodetachment well below 1 eV is evident from their spectrum and is assigned to the ${}^2D \rightarrow {}^3P$ transitions. However, the identification of actual thresholds is somewhat inconclusive; no final value for the 2D binding energy is given. Nevertheless, the Hotop-Lineberger tables from 1985 quote a value of 0.4(2) eV, which is apparently an estimate based on the work of Feldmann *et al.* For the 2D splitting an isoelectronically extrapolated value of 800(200) cm^{-1} is available [45]. The resulting energy level structure of Sn^- is shown in Fig. 14, including various photodetachment schemes aimed at the 2D_J levels.

The ionic ${}^4S_{3/2} \rightarrow {}^2D_{3/2,5/2}$ $M1$ transition probabilities are promising in this case; A coefficients of 0.2 and 0.01 s^{-1} , respectively, are obtained by extrapolating from calculated values of the Sb isoelectronic sequence [53], which translates into estimated counts per pulse of 10 and 0.5, respectively. We have searched for the ${}^4S_{3/2} \rightarrow {}^2D_J$ $M1$ resonances by scanning the two-photon detachment spectrum of $\text{Sn}^-({}^4S_{3/2})$ from high to low energies, starting at 7600 cm^{-1} . An enhancement in the signal of ~ 6 counts per pulse was found at 5762.50(10) cm^{-1} . This resonance feature is shown in Fig. 15 and must be assigned to the ${}^4S_{3/2} \rightarrow {}^2D_{3/2}$ transition on the basis of its strength. Apparently, the much weaker ${}^4S_{3/2} \rightarrow {}^2D_{5/2}$ transition had been missed. Therefore, an attempt was made at locating the ${}^2D_{5/2} \rightarrow {}^3P_{J'}$ thresholds.

A tin oxide instead of a tin metal cathode was utilized and found to perform much better at high effective sputter tem-

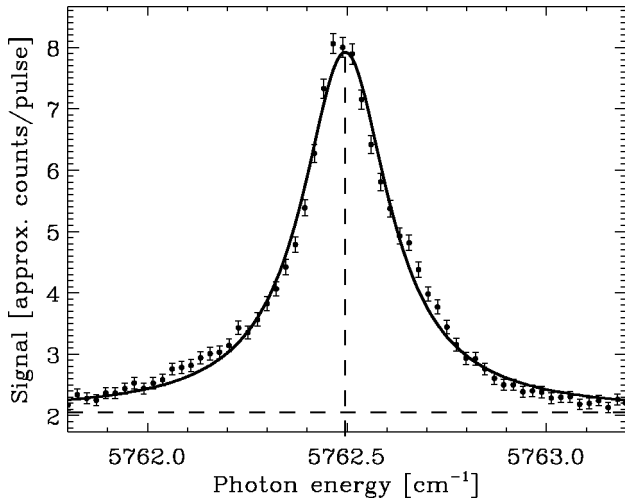


FIG. 15. Two-photon detachment yield of Sn in the vicinity of the ${}^4S_{3/2} \rightarrow {}^2D_{3/2}$ $M1$ resonance. The result of a Lorentzian fit to the data is indicated by the solid line.

peratures, albeit with a somewhat lower total Sn^- beam current of ~ 100 nA. The resulting increase in 2D population of over an order of magnitude now enabled a determination of four out of the five ${}^2D_J \rightarrow {}^3P_J$ thresholds with a reasonable signal-to-noise ratio. The ${}^2D_{5/2} \rightarrow {}^3P_2$ threshold is shown in Fig. 16 as an example. The threshold values that were obtained from Wigner s -wave fits to the four data sets are summarized in Table III. Binding energies of 3207.06(15) and 2457.04(10) cm^{-1} are obtained for ${}^2D_{3/2}$ and ${}^2D_{5/2}$, respectively, by subtracting from the threshold values the accurately known energies of the atomic 3P_J levels (0, 1691.806, and 3427.673 cm^{-1} [40]). It was now possible to zoom in on the thus far unobserved ${}^4S_{3/2} \rightarrow {}^2D_{5/2}$ $M1$ transition. The sum of several scans over a 1.5- cm^{-1} photon energy range is shown in Fig. 17. The weak but unambiguous resonance feature is centered at 6512.37(10) cm^{-1} . The resonant signal amounts to only 20% of the background signal, which is about a factor of 15 less than the signal-to-background ratio of the ${}^4S_{3/2} \rightarrow {}^2D_{3/2}$ resonance. This com-

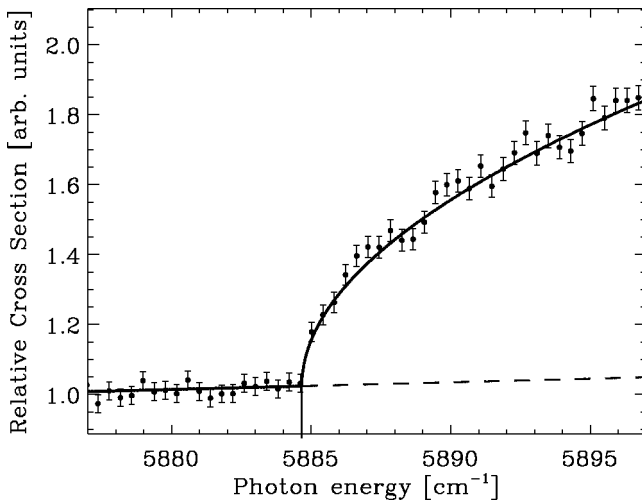


FIG. 16. Measured photodetachment cross section of Sn^- in the region of the ${}^2D_{5/2} \rightarrow {}^3P_2$ threshold. The result of a Wigner s -wave fit to the data is indicated by the solid line.

TABLE III. Results of the Wigner s -wave fits to the $\text{Sn}^-({}^2D)$ photodetachment data.

Transition	Threshold Energy (cm^{-1})	Binding energy of ionic level (cm^{-1})
${}^2D_{3/2} \rightarrow {}^3P_0$	3207.04(20)	3207.04(20)
${}^2D_{5/2} \rightarrow {}^3P_1$	4148.88(15)	2457.08(15)
${}^2D_{3/2} \rightarrow {}^3P_1$	4898.90(15)	3207.10(15)
${}^2D_{5/2} \rightarrow {}^3P_2$	5884.67(10)	2457.00(10)
${}^2D_{3/2} \rightarrow {}^3P_2$	a	a

^aThis threshold was not observed due to a small transition strength.

pares well with the ratio of ~ 20 for the extrapolated transition probabilities given above.

Finally, subtracting the measured resonance energies from the EA value yields a second set of ${}^2D_{3/2}$ and ${}^2D_{5/2}$ binding energies, 3206.93(15) and 2457.06(15) cm^{-1} , respectively, in excellent agreement with the values obtained from the threshold measurements. Based on the average of the two measurements we give final ${}^2D_{3/2}$ and ${}^2D_{5/2}$ binding energies of 3207.00(12) and 2457.05(12) cm^{-1} [397.617(15) and 304.635(15) meV], respectively, and a 2D_J splitting of 749.95(15) cm^{-1} .

The experimental results obtained here may be compared with the very recent relativistic configuration-interaction (RCI) calculations by O'Malley and Beck [54]. They report ${}^4S_{3/2} \rightarrow {}^2D_{3/2,5/2}$ splittings of 5903 and 6493 cm^{-1} , respectively, compared to our experimental values of 5762.48(10) and 6512.37(10) cm^{-1} . This is very satisfactory agreement, considering the complexity of the 51-electron system Sn^- . (Equally good agreement between measured and calculated level splittings was previously found in the case of Sb^- [16].)

The RCI calculation of O'Malley and Beck also provided $M1$ transition probabilities of 0.744 and 0.00420 s^{-1} for ${}^4S_{3/2} \leftarrow {}^2D_{3/2,5/2}$, respectively [54]. These $M1$ transition probabilities strongly depend on a small ($\sim 0.1\%$) admixture

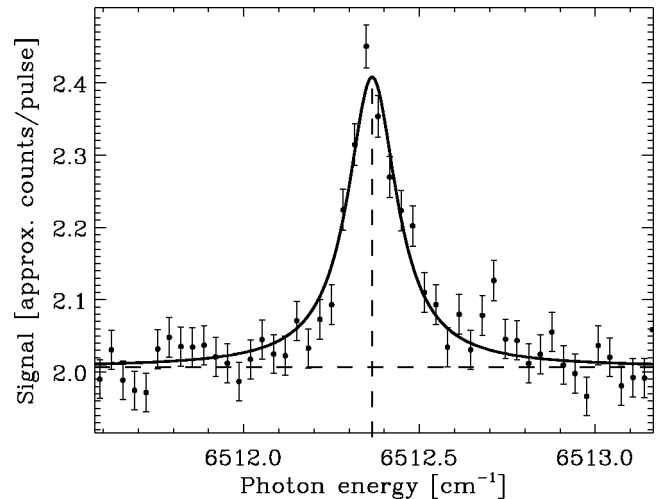


FIG. 17. Two-photon detachment yield of Sn in the vicinity of the ${}^4S_{3/2} \rightarrow {}^2D_{5/2}$ $M1$ resonance. The solid line represents a Lorentzian fit. Each data point corresponds to the signal from 3000 laser pulses.

TABLE IV. Summary of measured binding energies and fine structure splittings.

$^4S_{3/2}$ binding energy (eV)				
Ion	This work	Previous works	Ref.	
C ⁻	1.262119(20)	1.2629(3)	[5]	
Si ⁻	1.389521(20)	1.38949(6)	[47]	
Ge ⁻	1.232712(15)	1.23273(5)	[47]	
Sn ⁻	1.112067(15)	1.11209(6)	[47]	
Pb ⁻	a	0.364(8)	[56]	
2D binding energies (eV)				
Ion	This work		Previous works	Ref.
	$J=3/2$	$J=5/2$	(term average)	
C ⁻	a	a	0.033(1)	[5]
Si ⁻	0.527234(25)	0.525489(20)	0.523(5)	[46]
Ge ⁻	0.40144(10)	0.37757(6)	0.4(2)	[4]
Sn ⁻	0.397617(15)	0.304635(15)	0.4(2)	[4]
2D fine-structure splitting (cm ⁻¹)				
Ion	Measured	Extrapolated		Ref.
C ⁻	a	3(1)		[45]
Si ⁻	14.08(20)	7(2)		[45]
Ge ⁻	192.6(9)	160(30)		[45]
Sn ⁻	749.95(15)	800(200)		[45]

^aCould not be measured in the present study.

of $^2D_{3/2}$ into the $^4S_{3/2}$ state. With this in mind, they have revised their transition rates by more carefully treating the correlation of the $^2D_{3/2}$ level in the calculation of the $^4S_{3/2}$ wave function. They report revised $M1$ rates of 0.0791 and 0.004 31 s⁻¹ as well as $E2$ rates of 0.003 49 and 0.005 91 s⁻¹ for $^4S_{3/2} \leftarrow ^2D_{3/2,5/2}$, respectively [55]. Based on these numbers, which are somewhat smaller than the isoelectronically extrapolated values given above, the two transitions should differ in strength by a factor of 8, whereas an intensity ratio of 15 is observed.

E. Summary and outlook

The results of our infrared photodetachment studies of the carbon group negative ions C⁻, Si⁻, Ge⁻, and Sn⁻ are summarized in Table IV. Values obtained in previous experimental investigations or isoelectronically extrapolated values are given for comparison. The negative ion of lead, the last element in the carbon group, was not investigated here. Pb⁻ beams are very difficult to produce with a cesium sputter source. In various attempts with lead metal as well as lead oxide cathodes we were not able to produce more than ~10 pA of Pb⁻, which was insufficient for a determination of the EA-defining $^4S_{3/2} \rightarrow ^3P_0$ threshold. However, the EA of lead has been measured previously [56] and the 2D and 2P terms of Pb⁻ are expected to be unstable, on the basis of isoelectronic extrapolation. Hence highly accurate binding

energies are now available for almost all stable states of the carbon group negative ions. The remaining exceptions are the C⁻ (2D_J), Si⁻ (2P_J), and Pb⁻ ($^4S_{3/2}$) levels. As outlined earlier, these levels could be measured via infrared photodetachment threshold spectroscopy if alternative ion-beam production techniques such as charge exchange, and possibly state-selective detection schemes were utilized (discussed in detail in Ref. [22]).

In terms of multiphoton detachment, the observation of the $^4S_{3/2} \rightarrow ^2D_{5/2}$ resonance in Sn⁻ has demonstrated that laser-driven transitions into metastable ionic levels with radiative lifetimes as long as ~100 s are currently possible. Different storage rings (e.g., ELISA in Aarhus, Denmark) may in fact enable accurate lifetime measurements of such long-lived ionic states. Further improved or alternative tunable infrared laser sources such as optical parametric oscillators may provide wider tuning ranges, higher repetition rates, and/or more energetic pulses. Somewhat shorter pulses, say, 100 ps, could provide higher intensities and thus increase the probabilities of nonlinear processes, without additional spectral broadening. In some of the cases investigated here, resonant enhancements in multiphoton detachment spectra were expected on the basis of computer simulations, but not observed due to a substantial photodetachment background from excited ionic levels. In such cases, a strong laser pulse could be employed to deplete the excited level population of the ion beam via saturation detachment, before the ion beam is electrostatically deflected into the interaction region where the actual multiphoton detachment takes place. So far, multiphoton experiments that were aimed at excited states of atomic negative ions all employed photons in the optical regime. However, many possibilities seem to exist for resonant detachment schemes that involve photons of very different frequencies, e.g., in the optical and microwave regime. Combinations of laser and microwave sources have been successfully used in the past to study the hyperfine structure of $^{33}\text{S}^-$ [57] and the threshold detachment of S⁻ and Cl⁻ [42].

IV. CONCLUSION

This article has presented the results of a spectroscopic study of the C⁻, Si⁻, Ge⁻, and Sn⁻ ions. A tunable infrared laser source and a combination of single- and multiphoton detachment schemes were employed to very accurately determine most of the stable states of these ions ($\sigma < 0.1$ meV). The C⁻ (2D_J) and Si⁻ (2P_J) fine-structure splittings now remain the only undetermined structural features of the five carbon group negative ions.

ACKNOWLEDGMENTS

We gratefully acknowledge the Natural Science and Engineering Research Council of Canada (NSERC) for their support of this work. We also wish to thank J. D. Garrett for manufacturing the various sputter cathodes.

- [1] C. Blondel, Phys. Scr. **T58**, 31 (1995).
- [2] D. R. Bates, Adv. At., Mol., Opt. Phys. **27**, 1 (1991); T. Andersen, Phys. Scr. **T34**, 23 (1991).
- [3] S. J. Buckmann and C. W. Clark, Rev. Mod. Phys. **66**, 539 (1994); T. Andersen, H. H. Andersen, P. Balling, P. Kristensen, and V. V. Petrunin, J. Phys. B **30**, 3317 (1997).
- [4] H. Hotop and W. C. Lineberger, J. Phys. Chem. Ref. Data **14**, 731 (1985).
- [5] D. Feldmann, Z. Phys. A **277**, 19 (1976).
- [6] M. Scheer, R. C. Bilodeau, and H. K. Haugen, Phys. Rev. Lett. **80**, 2562 (1998).
- [7] M. Scheer, R. C. Bilodeau, J. Thøgersen, and H. K. Haugen, Phys. Rev. A **57**, R1493 (1998).
- [8] J. L. Hall, E. J. Robinson, and L. M. Branscomb, Phys. Rev. Lett. **14**, 1013 (1965).
- [9] W. C. Lineberger and T. A. Patterson, Chem. Phys. Lett. **13**, 40 (1972).
- [10] M. D. Davidson, H. G. Muller, and H. B. van Linden van den Heuvell, Phys. Rev. Lett. **67**, 1712 (1991); H. Stapelfeldt, P. Balling, C. Brink, and H. K. Haugen, *ibid.* **67**, 1731 (1991); C. Blondel, M. Crance, C. Delsart, and A. Giraud, J. Phys. B **24**, 3575 (1991).
- [11] R. Trainham, G. D. Fletcher, and D. J. Larson, J. Phys. B **20**, L777 (1987).
- [12] C. Y. Tang *et al.*, Phys. Rev. Lett. **66**, 3124 (1991).
- [13] R. Trainham, G. D. Fletcher, N. B. Mansour, and D. J. Larson, Phys. Rev. Lett. **59**, 2291 (1987); M. D. Davidson, J. Wals, H. G. Muller, and H. B. van Linden van den Heuvell, *ibid.* **71**, 2192 (1993).
- [14] P. Kristensen *et al.*, Phys. Rev. Lett. **71**, 3435 (1993); J. Thøgersen *et al.*, Phys. Rev. A **53**, 3023 (1996).
- [15] J. Thøgersen, M. Scheer, L. D. Steele, H. K. Haugen, and W. P. Wijesundera, Phys. Rev. Lett. **76**, 2870 (1996).
- [16] M. Scheer, H. K. Haugen, and D. R. Beck, Phys. Rev. Lett. **79**, 4104 (1997).
- [17] H. Stapelfeldt *et al.*, Phys. Rev. A **50**, 1618 (1994).
- [18] A. Stintz *et al.*, Phys. Rev. Lett. **75**, 2924 (1995).
- [19] V. K. Ivanov and L. P. Krukovskaya, J. Phys. B **27**, 4111 (1994); C. A. Ramsbottom, K. L. Bell, and K. A. Berrington, *ibid.* **26**, 4399 (1993); G. F. Gribakin, A. A. Gribakina, B. V. Gul'tsev, and V. K. Ivanov, *ibid.* **25**, 1757 (1992).
- [20] P. Balling, P. Kristensen, H. Stapelfeldt, T. Andersen, and H. K. Haugen, J. Phys. B **26**, 3531 (1993).
- [21] G. Haefliger, D. Hanstorp, I. Yu Kiyani, U. Ljungblad, H. H. Andersen, and T. Andersen, J. Phys. B **29**, 3017 (1996).
- [22] M. Scheer, C. A. Brodie, R. C. Bilodeau, and H. K. Haugen, Phys. Rev. A **58**, 2051 (1998).
- [23] W. K. Bischel and M. J. Dyer, Phys. Rev. A **33**, 3113 (1986); E. C. Looi, J. C. Stryland, and H. L. Welsh, Can. J. Phys. **56**, 1102 (1978), and references therein.
- [24] R. Middleton, Nucl. Instrum. Methods Phys. Res. **214**, 139 (1983).
- [25] E. P. Wigner, Phys. Rev. **73**, 1002 (1948).
- [26] J. W. Farley, Phys. Rev. A **40**, 6286 (1989); T. F. O'Malley, Phys. Rev. **137**, A1668 (1964).
- [27] R. C. Bilodeau, M. Scheer, and H. K. Haugen, J. Phys. B **31**, 3885 (1998).
- [28] P. C. Engelking and W. C. Lineberger, Phys. Rev. A **19**, 149 (1979).
- [29] L. Minnhagen, J. Opt. Soc. Am. **63**, 1185 (1973).
- [30] J. R. Nestor, Appl. Opt. **21**, 4154 (1982).
- [31] D. M. Neumark, K. R. Lykke, T. Andersen, and W. C. Lineberger, Phys. Rev. A **32**, 1890 (1985).
- [32] R. A. Bennett and J. L. Hall (unpublished). The results are quoted in Ref. [33].
- [33] D. Feldmann, Chem. Phys. Lett. **47**, 338 (1977).
- [34] V. A. Oparin, R. N. Il'in, I. T. Serenkov, and E. S. Solov'ev, Zh. Èksp. Teor. Fiz. **66**, 2008 (1974) [Sov. Phys. JETP **39**, 989 (1974)].
- [35] G. Haefliger, D. Hanstorp, I. Kiyani, A. E. Klingmuller, and U. Ljungblad, Phys. Rev. A **53**, 4127 (1996).
- [36] T. Noro, M. Yoshimine, M. Sekiya, and F. Sasaki, Phys. Rev. Lett. **66**, 1157 (1991); K. Raghavachari, J. Chem. Phys. **82**, 4142 (1985); R. A. Kendall, T. H. Dunning, Jr., and R. J. Harrison, *ibid.* **96**, 6796 (1992).
- [37] C. Froese Fischer, J. Phys. B **26**, 855 (1993).
- [38] C. Froese Fischer, A. Ynnerman, and G. Gaigalas, Phys. Rev. A **51**, 4611 (1995).
- [39] E. R. Cohen and B. N. Taylor, Rev. Mod. Phys. **59**, 1121 (1987).
- [40] E. B. Saloman, Spectrochim. Acta B **45**, 37 (1990); **47**, 517 (1992).
- [41] N. D. Gibson, B. J. Davies, and D. J. Larson, Phys. Rev. A **47**, 1946 (1993); C. H. Greene and N. Rouze, Z. Phys. D **9**, 219 (1988); P. Frey, F. Breyer, and H. Hotop, J. Phys. B **11**, L589 (1978).
- [42] M. C. Baruch, W. G. Sturru, N. D. Gibson, and D. J. Larson, Phys. Rev. A **45**, 2825 (1992).
- [43] D. J. Pegg, C. Y. Tang, J. Dellwo, and G. D. Alton, J. Phys. B **26**, L789 (1993).
- [44] D. H. Lee, W. D. Brandon, D. J. Pegg, and D. Hanstorp, Phys. Rev. A **56**, 1346 (1997).
- [45] H. Hotop and W. C. Lineberger, J. Phys. Chem. Ref. Data **4**, 539 (1975).
- [46] A. Kasdan, E. Herbst, and W. C. Lineberger, J. Chem. Phys. **62**, 541 (1975).
- [47] J. Thøgersen, L. D. Steele, M. Scheer, C. A. Brodie, and H. K. Haugen, J. Phys. B **29**, 1323 (1996).
- [48] D. Calabrese, A. M. Covington, J. S. Thompson, R. W. Marawar, and J. W. Farley, Phys. Rev. A **54**, 2797 (1996).
- [49] C. Mendoza and C. J. Zeippen, Mon. Not. R. Astron. Soc. **194**, 1 (1981).
- [50] T. M. Miller, A. E. Stevens Miller, and W. C. Lineberger, Phys. Rev. A **33**, 3558 (1986).
- [51] D. Feldmann, R. Rackwitz, E. Heinicke, and H. J. Kaiser, Z. Naturforsch. A **32A**, 302 (1977).
- [52] E. Biémont and J. E. Hansen, Phys. Scr. **33**, 117 (1986).
- [53] E. Biémont, J. E. Hansen, P. Quinet, and C. J. Zeippen, Astron. Astrophys., Suppl. Ser. **111**, 333 (1995).
- [54] S. M. O'Malley and D. R. Beck, Phys. Rev. A **57**, 1743 (1998).
- [55] S. M. O'Malley and D. R. Beck (private communication).
- [56] C. S. Feigerle, R. R. Corderman, and W. C. Lineberger, J. Chem. Phys. **74**, 1513 (1981).
- [57] R. Trainham, R. M. Jopson, and D. J. Larson, Phys. Rev. A **39**, 3223 (1989).